



室蘭工業大学

学術資源アーカイブ

Muroran Institute of Technology Academic Resources Archive



Single-polarization hollow-core square photonic bandgap waveguide

メタデータ	言語: en 出版者: American Institute of Physics (AIP) 公開日: 2016-11-28 キーワード (Ja): キーワード (En): 作成者: 江口, 真史, 辻, 寧英 メールアドレス: 所属:
URL	http://hdl.handle.net/10258/00009067

This work is licensed under a Creative Commons Attribution 4.0 International License.





Single-polarization hollow-core square photonic bandgap waveguide

Masashi Eguchi and Yasuhide Tsuji

Citation: *AIP Advances* **6**, 075322 (2016); doi: 10.1063/1.4960426

View online: <http://dx.doi.org/10.1063/1.4960426>

View Table of Contents: <http://scitation.aip.org/content/aip/journal/adva/6/7?ver=pdfcov>

Published by the *AIP Publishing*

Articles you may be interested in

[Gas refractometry using a hollow-core photonic bandgap fiber in a Mach-Zehnder-type interferometer](#)
Appl. Phys. Lett. **100**, 051106 (2012); 10.1063/1.3681171

[Near-Infrared Raman Spectroscopy Using Hollow-Core Photonic Bandgap Fibers](#)
AIP Conf. Proc. **1267**, 780 (2010); 10.1063/1.3482806

[Hollow-core resonator based on out-of-plane two-dimensional photonic band-gap crystal cladding at microwave frequencies](#)
Appl. Phys. Lett. **96**, 051108 (2010); 10.1063/1.3303857

[Tailoring the Nonlinear Response of Hollow-core Photonic Bandgap Fibres](#)
AIP Conf. Proc. **1055**, 54 (2008); 10.1063/1.3002542

[APL Photonics](#)

NEW Special Topic Sections

NOW ONLINE
Lithium Niobate Properties and Applications:
Reviews of Emerging Trends

AIP Applied Physics Reviews

Single-polarization hollow-core square photonic bandgap waveguide

Masashi Eguchi^{1,a} and Yasuhide Tsuji^{2,b}

¹*Department of Opto-Electronic System Engineering, Chitose Institute of Science and Technology, Chitose, 066-8655 Japan*

²*Division of Information and Electronic Engineering, Graduate School of Engineering, Muroran Institute of Technology, Muroran, 050-8585 Japan*

(Received 3 April 2016; accepted 18 July 2016; published online 29 July 2016)

Materials with a periodic structure have photonic bandgaps (PBGs), in which light can not be guided within certain wavelength ranges; thus light can be confined within a low-index region by the bandgap effect. In this paper, rectangular-shaped hollow waveguides having waveguide-walls (claddings) using the PBG have been discussed. The design principle for HE modes of hollow-core rectangular PBG waveguides with a Bragg cladding consisting of alternating high- and low-index layers, based on a 1D periodic multilayer approximation for the Bragg cladding, is established and then a novel single-polarization hollow-core square PBG waveguide using the bandgap difference between two polarized waves is proposed. Our results demonstrated that a single-polarization guiding can be achieved by using the square Bragg cladding structure with different layer thickness ratios in the mutually orthogonal directions and the transmission loss of the guided mode in a designed hollow-core square PBG waveguide is numerically estimated to be 0.04 dB/cm. © 2016 Author(s). All article content, except where otherwise noted, is licensed under a Creative Commons Attribution (CC BY) license (<http://creativecommons.org/licenses/by/4.0/>). [<http://dx.doi.org/10.1063/1.4960426>]

I. INTRODUCTION

Photonic crystal waveguides with periodic structures in the cladding and/or core regions have the potential of achieving various novel properties that are quite impossible in conventional waveguides, and have been studied actively from the mid 1990s.¹ In particular, photonic bandgap (PBG) effects caused by a periodic modulation of refractive index prohibit the propagation of light of certain frequencies, and thus PBG fibers/waveguides based on the PBG confinement² can open up a possibility for trapping light in low-index regions and enable air-guiding that is impossible in conventional waveguides relying on index guiding. The air-guiding is attractive for ultra-low loss transmission because it can ultimately reduce the core material loss. In addition, because of the high heat resistance and extremely low nonlinearity of the core material (i.e., air), the PBG waveguides are suitable for high power delivery. They have also been applied to the field of optofluidics.

Various hollow-core PBG fibers with a coaxial periodic cladding³⁻⁵ and two-dimensional (2D) periodic cladding⁶⁻⁸ have been reported to date. Additionally, absolutely single-polarization PBG fibers, which can guide only one polarization state of the doubly degenerate fundamental mode, have been proposed.⁹⁻¹² Polarization-maintaining or single-polarization fibers are required in the fields of telecommunication, measurement, and sensing, such as polarization multiplexing/polarization multiplexed bi-directional transmissions, optical interferometric systems (e.g., interferometric fiber-optic sensors), and connections to polarization strongly dependent photonic integrated circuits. Compared to axisymmetric circular fibers and photonic crystal fibers with sixfold rotational symmetry¹³ consisting of air holes arranged in a triangular lattice, in which the fundamental mode

^aElectronic mail: Corresponding author: megu@ieee.org

^bElectronic mail: y-tsuji@mmm.muroran-it.ac.jp



is doubly degenerate, waveguides with a rectangular cross-section are excellent in polarization-preserving capability.

In this work, we establish the design principle of hollow-core rectangular PBG waveguides with a Bragg cladding consisting of one-dimensional (1D) periodically stratified dielectric films, whose design for HE modes has not been reported in detail to date, demonstrate its effectiveness by designing hollow-core rectangular PBG waveguides, and then propose a novel single-polarization hollow-core square PBG waveguide using the bandgap difference between two polarized waves. A kind of rectangular waveguides using the Bragg reflection caused by periodically stratified dielectric films have already been reported in Refs. 14–17; these waveguides are implemented on photonic integrated circuits. The hollow waveguides presented in Ref. 14 have a hollow core, to be sure, but they have a Bragg confinement structure only in the vertical direction and not in the horizontal direction, and thus seem to be close to slab waveguides in terms of spatial light confinement. By contrast, although those in Refs. 15 and 16 have a rectangular cladding with a multilayer-like structure, their cores are made of a solid material, not hollow. In all these papers, TE and TM modes are considered as their guided modes, but such waveguide structures with a rectangular-like core surrounded by Bragg stacks do not support pure TE and TM modes but hybrid modes. In Ref. 17, a hollow-core Bragg waveguide with a cladding shape close to a rectangular was fabricated. However, the design of hollow-core *circular* Bragg fibers has been discussed there; these fibers have been regarded as an air-guiding layer slab waveguide with a Bragg stack cladding by assuming a large diameter and their modal properties have been predicted using the TE and TM modes of the approximated slab waveguide. In addition, to the best of our knowledge, square core waveguides supporting single-polarization guiding have never been reported before.

In order to obtain the PBG guidance of the HE modes of hollow-core rectangular PBG waveguides with a Bragg stack cladding, we devise the design principle based on the bandgap estimation of their rectangular Bragg claddings using the approximated 1D periodic dielectric films. Thus, first the polarization-dependent property of the PBG of 1D periodic multilayer media, which is required for the bandgap estimation, is systematically studied for the conditions of wave propagation and the structural parameters in detail. Next, a hollow-core rectangular PBG waveguide using the omnidirectional Bragg reflection caused by the multilayer cladding wall is designed based on the results. Finally, by using the polarization anisotropy in the PBG of periodic multilayers, a novel single-polarization hollow-core square PBG waveguide with relatively low loss that supports only one polarization state is designed.

II. HOLLOW-CORE RECTANGULAR PHOTONIC BANDGAP WAVEGUIDE AND THE BRAGG CLADDING

A hollow-core rectangular PBG waveguide is a rectangular waveguide having Bragg stack waveguide-walls, which consist of periodically stratified dielectric films as shown in Fig. 1(a). Figure 1(b) shows the structure of the Bragg cladding consisting of alternating layers of low and high refractive indices. Since this cladding structure does not have an exactly periodic structure for z -directed waves as a whole 2D cross section, the hollow-core rectangular PBG waveguide shown in Fig. 1 does not rigorously support eigen-modes. Nevertheless, guided modes with strong light confinement can be designed depending on the waveguide structure and the propagation angle of waves.

Periodically stratified dielectric films possess a PBG effect, by which light can not be guided within certain wavelength ranges, and the bandgap difference between two polarized waves occurs for obliquely propagating waves. Many research efforts have thus far been devoted to 1D multilayer dielectric stacks; most of them have focused on attaining broadband, polarization-independent, and omnidirectional reflections for low loss multilayer dielectric mirrors and interference filters. In order to make use of the Bragg reflection caused by the PBG, it is desirable that the bandgap width be as large as possible. In addition, a large polarization anisotropy of the bandgap is required for designing the hollow-core PBG waveguides discussed here. In this section, to design hollow-core PBG waveguides with a rectangular Bragg stack waveguide-wall, the bandgap properties, especially

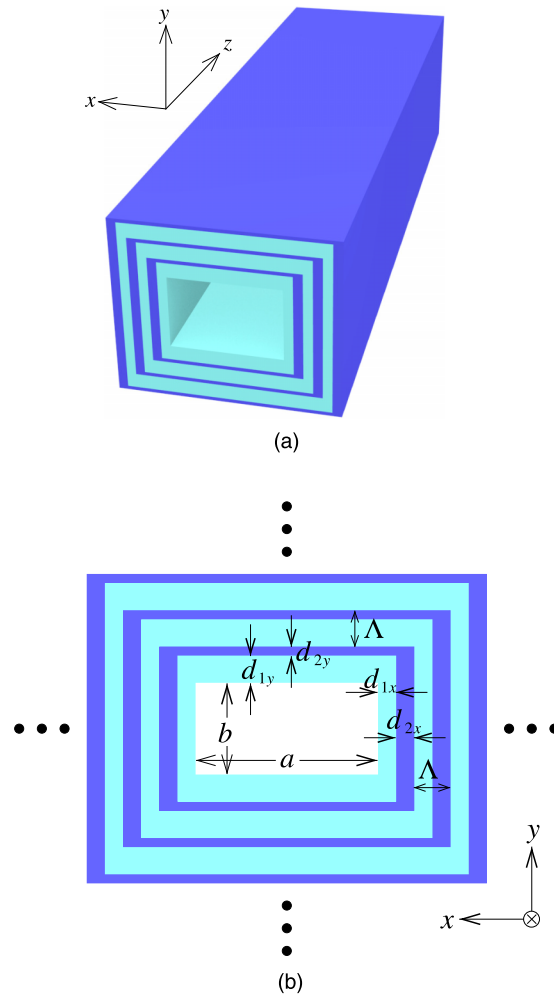


FIG. 1. Hollow-core rectangular photonic bandgap waveguide. (a) Waveguide structure. (b) Bragg cladding.

bandgap width and polarization-dependent property, of the PBG of periodic multilayer media are systematically investigated and summarized.

Our structural design for hollow-core rectangular PBG waveguides, which is presented in Section III, is based on the bandgap properties of periodic multilayer structures. An ideal bandgap is obtained only in infinite periodic structures as shown in Fig. 2(a), while only a finite number of periodic layers as shown in Fig. 2(b) are practically available to us. Hence, the bandgap analysis of finite periodic multilayer structures is required for accurately designing these waveguides. However, the approximate estimation of the bandgaps will be obtained from the bandgap calculations using infinite periodic structures. The wave propagation in infinite or finite periodic multilayer media can be calculated by a transfer matrix method.^{18–20} Nevertheless, since this calculation constitutes the core of our design principle, an overview of the method is given in Appendix.

A. BANDGAP PROPERTY OF PERIODIC STRATIFIED MEDIA: OBLIQUELY PROPAGATING WAVES

We begin by considering the bandgap property of periodic multilayer stacks with a period of length $\Lambda = d_1 + d_2$ with a uniform layer thickness ($d_1 : d_2 = 1 : 1$), as shown in Fig. 2(a). The refractive indices of the alternating low- and high-index layers are assumed to be $n_1 = 1.45$ and

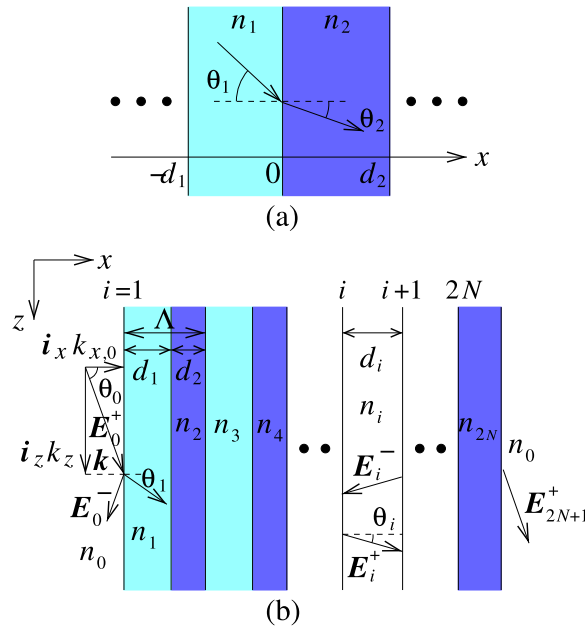


FIG. 2. 1D multilayer structure. (a) Unit cell of an infinite periodic multilayer structure. (b) Multilayer structure with a finite number of layers composed of $2N$ layers.

$n_2 = 3.4$, respectively, throughout in this paper. These values correspond to a refractive index of silica and silicon, respectively. For the finite periodic structure shown in Fig. 2(b), (n_1, d_1) and (n_2, d_2) correspond to layers with odd and even indices i , respectively (see Eq. (A20)). The plane waves propagating in the xz plane of the multilayer medium, as shown in Figs. 2(a) and 2(b), are classified as TE (s) and TM (p) waves, which have only one electric-field and magnetic-field components, respectively, in the plane of the films. While the polarization anisotropy of bandgap between TE and TM waves does not exist for vertical propagation ($\theta_0 = \theta_1 = \theta_2 = 0$), it occurs for oblique propagation. Here, we clarify the polarization anisotropy in the bandgap of periodic multilayer structures for obliquely propagating waves. In infinite periodic structures, the bandgap for obliquely propagating waves is obtained from Eq. (B3) and shown in Fig. 3. The light- and dark-shaded regions indicate the bandgaps for TE, and both TE and TM waves, respectively, the vertical axis represents the normalized wavenumber k_z/k_0 tangential to the layer surfaces (see Appendix for k_z and k_0), and λ is the free-space wavelength. The bandgap for the TE (s) wave contains that for the TM (p) wave and thus, this is used in Bragg mirrors to achieve omnidirectional reflections.^{21–23} The wavenumbers at which the bandgaps for TM waves close correspond to Brewster’s angle ($k_z/k_0 = 1.3338$). However, for waves incident from a low-index external material, the tangential wavenumber components

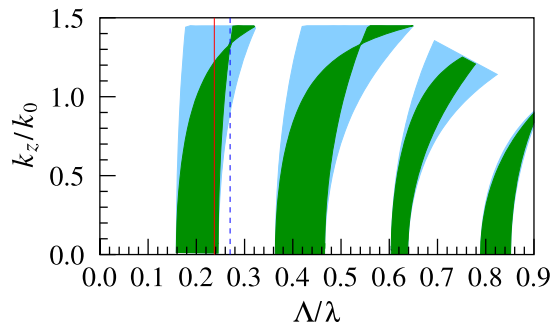


FIG. 3. Bandgap for oblique propagation waves in an infinite periodic multilayer stack with $n_1 = 1.45$, $n_2 = 3.4$, and $d_1 : d_2 = 1 : 1$. The light- and dark-shaded regions indicate the PBGs for TE, and both TE and TM waves, respectively. Red-colored solid line: $\Lambda/\lambda = 0.2381$, blue-colored dashed line: $\Lambda/\lambda = 0.2703$.

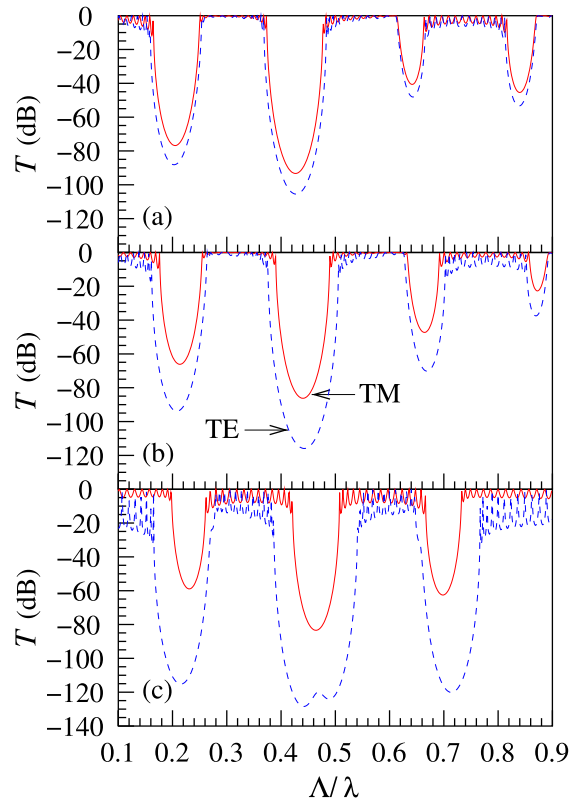


FIG. 4. Transmission coefficient of finite periodic multilayer films with 15 periods ($d_1 : d_2 = 1 : 1$, $n_1 = 1.45$, and $n_2 = 3.4$) for oblique incident waves. (a) $k_z/k_0 = 0.5$. (b) 0.75. (c) 0.995.

satisfying the Brewster condition for the multilayer structure are beyond their range limited by the critical angle for the interface between the external and first layer materials, e.g., $0 \leq k_z/k_0 \leq 1$ for incident waves from the air.

Next, in Fig. 4, we show the transmission coefficient for the propagation of waves obliquely incident on finite periodic multilayer films. Since an increase in the number of layer periods leads to the forbidden band (or stopband) close to that of infinite periodic structure, here the number of periods was considered to be $N = 15$. Figures 4(a), 4(b), and 4(c) display the transmission coefficients in normalized tangential wavenumbers of 0.5, 0.75, and 0.995, respectively, corresponding to $\theta_0 = 30, 48.59,$ and 84.27° . The dashed and solid curves in these figures correspond to TE and TM waves, respectively. Forbidden bands corresponding to the PBG of infinite periodic structures appear in the transmission coefficient. We can see that, as with the infinite periodic structure, the bandgap difference between the two polarized waves increases with the tangential wavenumber k_z/k_0 corresponding to the propagation angle. The bandgap for TE waves increases with the tangential wavenumber, whereas that for TM waves gets narrower. We also see that the bandgaps for both polarized waves shift toward the blue side with an increase in the tangential wavenumber and the transmission coefficients in their passbands are found to drop.^{21,22,24} Additionally, the oscillation in the passbands originates from the Fresnel reflections at each layer interface.

B. BANDGAP PROPERTY OF PERIODIC STRATIFIED MEDIA: LAYER THICKNESS RATIO

The bandgap property of 1D periodic multilayer structures can be controlled by their structural parameters, including the refractive index and thickness of layers. The layer thickness generally allows more flexibility in the design than the refractive index of layer. In this section, the polarization-dependent bandgap for layer thickness ratios is elucidated. Figures 5(a), 5(b), 5(c), and 5(d) display the bandgap properties for $k_z/k_0 = 0.995$ of periodic multilayer films with 15

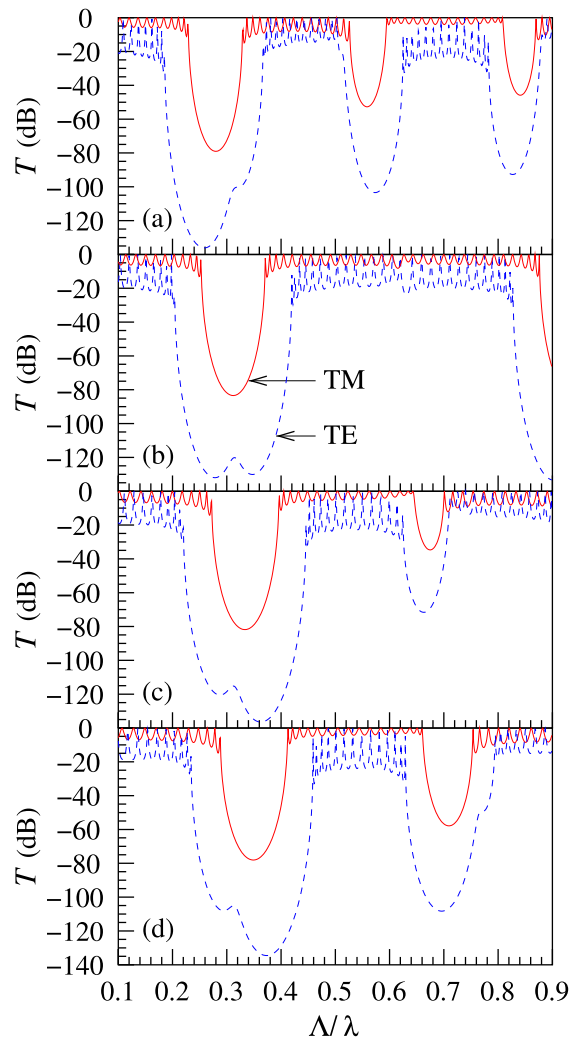


FIG. 5. Transmission coefficient of finite periodic multilayer films with 15 periods for the thickness of low-index layer for $k_z/k_0 = 0.995$. (a) $d_1 : d_2 = 2 : 1$. (b) $d_1 : d_2 = 3 : 1$. (c) $d_1 : d_2 = 4 : 1$. (d) $d_1 : d_2 = 5 : 1$.

periods for layer thickness ratios of $d_1 : d_2 = 2 : 1$, $3 : 1$, $4 : 1$, and $5 : 1$, respectively. Here, the period length Λ is assumed to be a constant value. Since d_1 and d_2 correspond to the thicknesses of low- and high-index layers, respectively, the bandgap shifts toward the blue side, and the bandgap width for TE waves and the bandgap difference between both polarizations gradually increase as the low-index layer thickness increases. In addition, when approximately $d_1 : d_2 = 4 : 1$, the bandgap for TM waves is completely deviated from that for $d_1 : d_2 = 1 : 1$ shown in Fig. 4(c). In using bandgap effects, since it is desirable that the bandgap width is larger, the thickness of low-index layer should be larger than that of high-index layer.

Finally, the polarization-dependent bandgap of infinite periodic multilayer media for the layer thickness ratio is shown in Fig. 6. The dashed curve indicates the relative PBG width difference of the primary PBG defined as the difference in PBG width between TE and TM waves divided by the center frequency of PBG for TE waves. The bandgap property for the low-index layer thickness similar to the finite periodic multilayer stacks is observed and the maximum bandgap width can be seen to be located around $d_1 : d_2 = 4 : 1$ (more precisely, $d_1/\Lambda = 0.76$). In addition, regardless of polarization state, the higher-order bandgaps are observed to disappear for certain thickness ratios in the range of propagation angles smaller than Brewster's angle. A similar phenomenon can also be seen in the transmission property of a finite periodic multilayer stack with $d_1 : d_2 = 3 : 1$

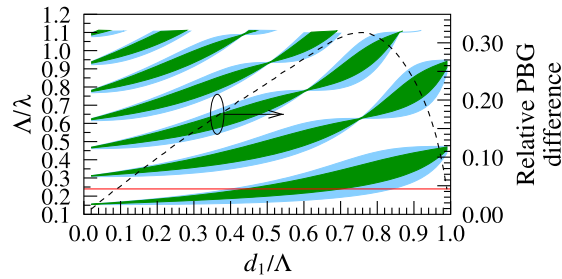


FIG. 6. Bandgap and relative PBG width difference of the primary PBG (dashed curve) of infinite periodic multilayer media as a function of the thickness of low-index layer for $k_z/k_0 = 0.995$. Red-colored solid line: $\Lambda/\lambda = 0.24$.

in Fig. 5(b), in which the second bandgap is observed to disappear. This is because, even under the Bragg condition, the reflected waves from the front face and the intermediate interface within a period segment are in opposite phase and thus cancel each other out. For instance, this layer thickness ratio for the second bandgap is given by

$$\frac{d_1}{\Lambda} = \left[1 + \frac{\sqrt{n_1^2 - (k_z/k_0)^2}}{\sqrt{n_2^2 - (k_z/k_0)^2}} \right]^{-1}, \quad (1)$$

is thus estimated to be 0.7550, and this is found to be in good agreement with that in the bandgap diagram shown in Fig. 6.

From the above results, it is apparent that the bandgap difference between both polarizations becomes larger as the low-index layer thickness increases relative to the high-index layer thickness. In addition, there is an optimum value of thickness ratio that maximizes the bandgap width. In the present study, since the refractive indices of the alternating low- and high-index layers are assumed to be $n_1 = 1.45$ and $n_2 = 3.4$, respectively, the bandgap width will reach its maximum at about $d_1 : d_2 = 4 : 1$.

III. DESIGN PRINCIPLE OF HOLLOW-CORE RECTANGULAR PHOTONIC BANDGAP WAVEGUIDE

The hollow-core rectangular PBG waveguides shown in Fig. 1(a) support the hybrid modes, referred to as HE modes. Here, we first present the design principle for HE modes of hollow-core rectangular PBG waveguides with a Bragg cladding, based on a 1D periodic multilayer approximation for the Bragg cladding, and attempt to design a hollow-core rectangular PBG waveguide using the omnidirectional Bragg reflection caused by its cladding.

In order to obtain a light confinement structure, the Bragg cladding must satisfy the PBG condition for propagation waves in the z direction shown in Fig. 1(a). While the rectangular Bragg cladding shown in Fig. 1(b) can be regarded as a 1D periodic structure in each of the x and y directions, it does not have an exactly periodic structure as a whole 2D cross section and thus a complete bandgap as in well-known 2D periodic air-hole lattice claddings can not be achieved for the cladding region. Nevertheless, it seems that adequate Bragg reflections can be obtained depending on the waveguide structure and the propagation angle of waves. Therefore, in this study, we regard the rectangular Bragg cladding as the respective 1D periodic multilayer films, which are stacked in each of the x and y directions, as shown in Figs. 7(a) and 7(b), and then estimate its quasi-bandgap using the respective bandgap properties in each direction. In Fig. 7, \mathbf{E} , \mathbf{H} , and \mathbf{k} represent the electric, magnetic field vectors, and wavevector, respectively. Rectangular metallic waveguides used in the microwave and millimeter-wave bands support only TE and TM modes, which have no longitudinal electric- and magnetic-field components, respectively. (It should be noted that the TE and TM modes in metallic waveguides are different from those in 1D layered structures.) On the other hand, the hollow-core rectangular waveguides with a periodic multilayer dielectric cladding shown

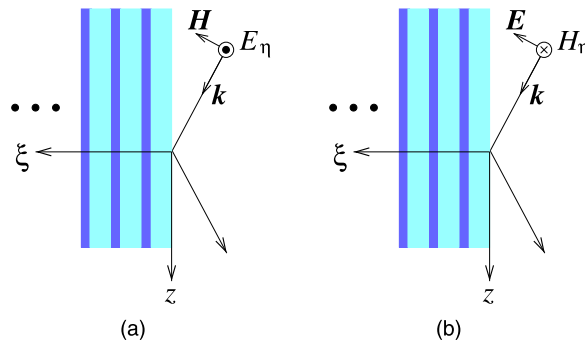


FIG. 7. Approximated 1D periodic multilayer films for Bragg cladding and TE- and TM-wave approximation. (a) TE(*s*)-wave approximation. (b) TM(*p*)-wave approximation.

in Fig. 1 can not guide pure TE and TM waves but hybrid waves being combinations of these waves, which have two polarized modes: *x*- and *y*-polarized modes having two dominant components E_x and H_y , and E_y and H_x , respectively. Here, we approximate the 2D rectangular Bragg cladding by the respective 1D periodic multilayer stacks along each axis and then, based on the dominant components, estimate the quasi-bandgap by approximating each polarized mode by either TE (*s*) or TM (*p*) wave for each direction, as shown in Fig. 7. For example, the *x*-polarized mode is approximated by the TM and TE waves, which have a magnetic- and electric-field components, respectively, in the plane of the films, corresponding to $(\xi, \eta) = (x, y)$ in Fig. 7(b) for the *x*-axis direction and $(\xi, \eta) = (y, x)$ in Fig. 7(a) for the *y*-axis direction, respectively, and vice versa for the *y*-polarized mode.

In Section II, we demonstrated the bandgap of an infinite periodic multilayer stack with a layer thickness ratio of $d_1 : d_2 = 1 : 1$ (Fig. 3). The vertical axis k_z/k_0 corresponds to the normalized wavenumber in the propagation direction, which is referred to as the effective index; thus $k_z/k_0 = 0$ indicates the bandgap for waves propagating perpendicular to the layer surfaces. As mentioned in Section II A, the bandgap for TE waves completely contains that for TM waves, and thus the complete bandgaps common to both TE and TM waves can be obtained within the frequency ranges satisfying the bandgaps for TM waves.

Here, we consider a hollow-core PBG waveguide with a square core with $a = b = 40\Lambda$. The number of guided modes (e.g., single-mode or few-mode or multi-mode guiding) can be approximately designed by the core size estimated based on the metallic waveguide theory. In order to calculate the guided modes, a 2D vector finite-element method²⁵ based on curvilinear edge/nodal hybrid elements is applied to one-quarter of the waveguide cross section, taking twofold symmetry into account. Figures 8(a) and 8(b) show the modal field distributions of the *x*- and *y*-polarized fundamental modes, respectively, which are denoted as HE_{11}^x and HE_{11}^y in the Marcattili notation,²⁶ at

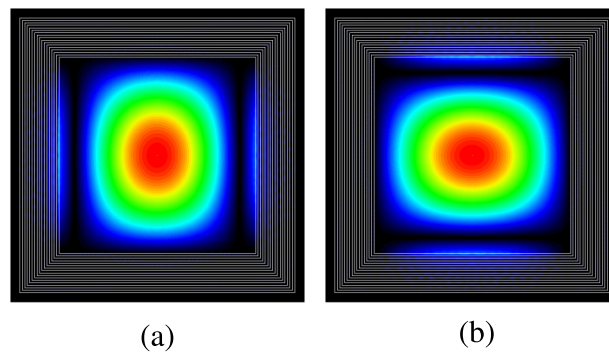


FIG. 8. Modal field of a hollow-core square PBG waveguide consisting of a core with $a = b = 40\Lambda$ and a Bragg cladding with $N = 8$ and $d_1 : d_2 = 1 : 1$ at $\Lambda/\lambda = 0.2381$. (a) *x*-polarized mode. (b) *y*-polarized mode.

$\Lambda/\lambda = 0.2381$. In these figures, the results for a Bragg cladding with the number of periods $N = 8$, in which a good light confinement was observed, have been displayed. As can be seen from the red-colored solid line in Fig. 3 corresponding to $\Lambda/\lambda = 0.2381$, the bandgap for TM wave is satisfied. Since, in a square core waveguide, the two polarized modes are degenerate, the fundamental mode can be seen to be well confined to the core region in both polarized modes. The effective indices of the x - and y -polarized modes were both 0.996691. The effective index of the TE₁₁ mode in a square metallic waveguide with the same core size is given by

$$n_{\text{eff}} = \sqrt{1 - \frac{1}{2} \frac{\lambda^2}{a^2}} = 0.997240. \quad (2)$$

There is a little difference between the effective indices of the hollow-core PBG and metallic waveguides. Figure 9 shows the modal field distribution at $\Lambda/\lambda = 0.2703$. As can be seen from the blue-colored dashed line in Fig. 3, this wave frequency is mostly out of the bandgaps for both polarized waves with an effective index below 1. Thus, outgoing radiation waves passing through the Bragg cladding are observed for $\Lambda/\lambda = 0.2703$ and the modes no longer are confined within the core.

IV. SINGLE-POLARIZATION HOLLOW-CORE SQUARE PHOTONIC BANDGAP WAVEGUIDE

A polarization controlled transmission can be achieved by using a rectangular shape even in the PBG waveguides using the omnidirectional Bragg reflection mentioned in Sec. III (and, of course, also in simple metallic rectangular waveguides, but they are not suitable for the optical wave band). However, a square shape is desirable for the waveguide core for practical use such as low-loss connection to standard fibers, photonic-crystal fibers, and other conventional waveguide devices. Therefore, we attempt to develop a hollow-core square PBG waveguide supporting single-polarization guiding. In 1D periodic multilayer structures, the TE and TM waves that are degenerate for vertical propagation become nondegenerate for oblique propagation, and thus the difference in PBG between two polarized waves occurs, as mentioned in Section II A. By making use of this polarization anisotropy of PBG, the single-polarization guiding that supports only one polarization state can be achieved. Here, we consider only x -polarized mode guiding and make use of the primary bandgap. The layer thickness ratios of the Bragg cladding, $d_{1x} : d_{2x}$ and $d_{1y} : d_{2y}$, are designed to satisfy the bandgaps for TM waves (corresponding to $(\xi, \eta) = (x, y)$ in Fig. 7(b)) and only for TE waves excluding that for TM waves (corresponding to $(\xi, \eta) = (y, x)$ in Fig. 7(a)) for the multilayer cladding walls stacked perpendicular to the x and y axes, respectively, which correspond to the dark- and light-shaded regions in Fig. 3. In this case, the Bragg condition is satisfied for the x -polarized modes in both x and y directions, but not for the y -polarized modes in the y direction, because the y -polarized waves are approximated by TM waves corresponding

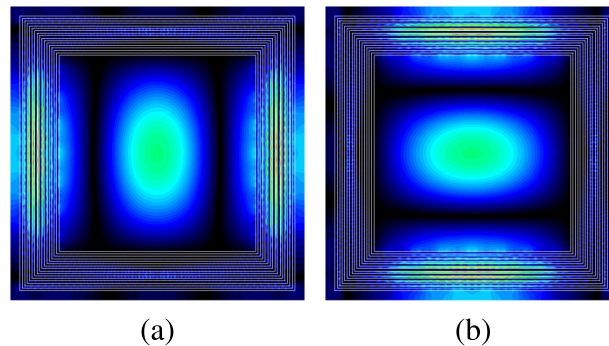


FIG. 9. Modal field of a hollow-core square PBG waveguide consisting of a core with $a = b = 40\Lambda$ and a Bragg cladding with $N = 8$ and $d_1 : d_2 = 1 : 1$ at $\Lambda/\lambda = 0.2703$. (a) x -polarized mode. (b) y -polarized mode.

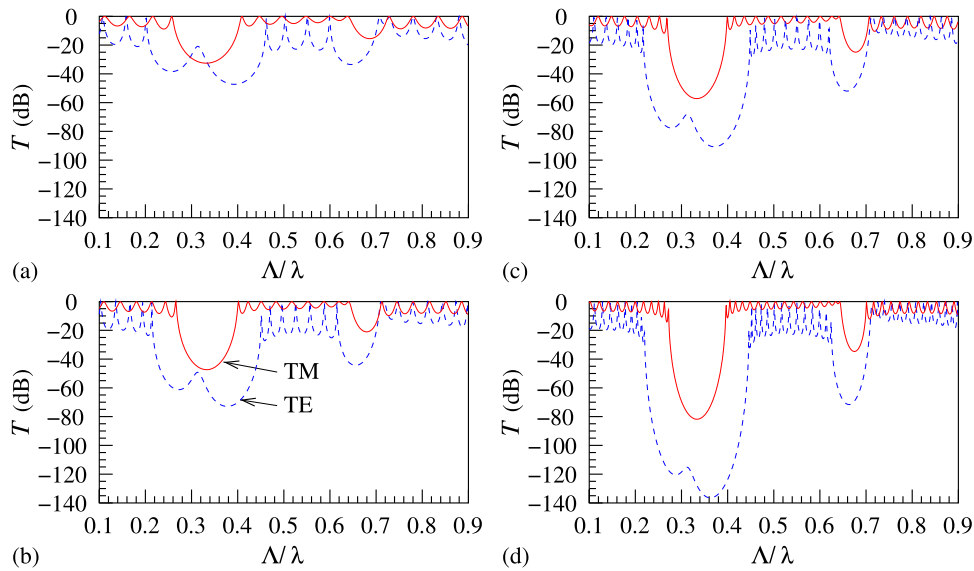


FIG. 10. Transmission coefficient T of finite periodic multilayer films with a thickness ratio of $d_1:d_2=4:1$ for $k_z/k_0=0.995$ in the case of different number of layer periods. (a) $N=5$ (b) $N=8$ (c) $N=10$ (d) $N=15$.

to $(\xi, \eta) = (y, x)$ in Fig. 7(b), in that direction. As a result, only the x -polarized modes can confine light in the core region. Thus, the periodic multilayer films satisfying the bandgap only for TE waves act as a polarization filter and, by using this principle, the single-polarization guiding can be achieved even for a square shaped core, which leads to the polarization mode degeneracy between the two orthogonally polarized modes in metallic hollow or dielectric waveguides.

For wider bandwidth operation, it is desirable that the difference between the bandgaps for TE and TM waves and the bandgap widths themselves be as large as possible. As mentioned in Section II, in periodic multilayer films the thicker low-index layer relative to the high-index layer and wave propagations with larger tangential wavenumbers lead to wider bandgap widths and larger bandgap differences between TE and TM waves. Figure 10 shows the transmission coefficient T of finite periodic multilayer films with a thickness ratio of $d_1:d_2=4:1$ for wave propagations with $k_z/k_0=0.995$ in the case of different number of layer periods N . Sufficiently wide bandgaps only for TE waves are obtained on both sides of the bandgaps for TM waves, because of the large propagation angle of traveling waves and the layer thickness ratio that approximately maximizes the bandgap widths.

Based on these results, the thickness ratio of the Bragg cladding wall stacked in the y direction is assumed to be $d_{1y}:d_{2y}=4:1$ and the normalized frequency Λ/λ is chosen to be 0.24, which is located within the bandgap only for TE waves. Meanwhile, the Bragg cladding wall stacked in the x direction must satisfy the bandgap for TM waves for the lateral confinement in the x direction. In Fig. 6, showing the layer thickness ratio dependence of the bandgap of infinite periodic multilayer stack, the red-colored solid line corresponds to $\Lambda/\lambda=0.24$. The range of layer thickness ratio falling within the bandgap for TM waves can be estimated from this figure and here we take $d_{1x}:d_{2x}=1:1$.

Figures 11 and 12 show the modal field distributions of the fundamental modes in hollow-core square PBG waveguides having a core with $a=b=40\Lambda$ and 5-period and 10-period Bragg claddings, respectively, with $d_{1x}=d_{2x}=0.5\Lambda$, $d_{1y}=0.8\Lambda$, and $d_{2y}=0.2\Lambda$. In the 5-period Bragg cladding, since the bandgap effect is small, the mode field is found not to be sufficiently confined to the core region not only in the y -polarized mode but also in the x -polarized mode; slight mode leakage out through the Bragg cladding in the x direction can be seen in the x -polarized mode, even though it is unclear in the figure. By contrast, the 10-period Bragg cladding provides a good confinement of the x -polarized mode, but also causes a slight confinement of the y -polarized mode, as can be seen in Fig. 12(b). This would result from the following reason. An increase in the number

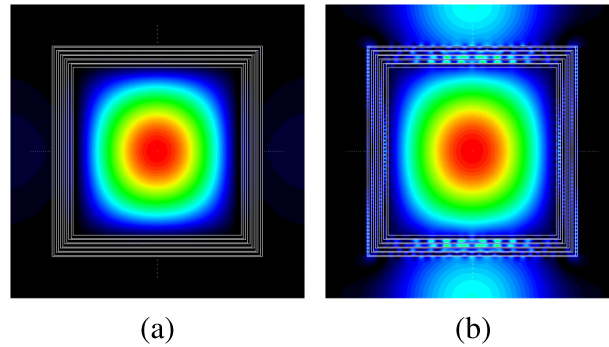


FIG. 11. Modal field of a single-polarization hollow-core square PBG waveguide consisting of a core with $a = b = 40\Lambda$ and a 5-period Bragg cladding ($d_{1x} = d_{2x} = 0.5\Lambda$, $d_{1y} = 0.8\Lambda$, and $d_{2y} = 0.2\Lambda$) at $\Lambda/\lambda = 0.24$. (a) x -polarized mode. (b) y -polarized mode.

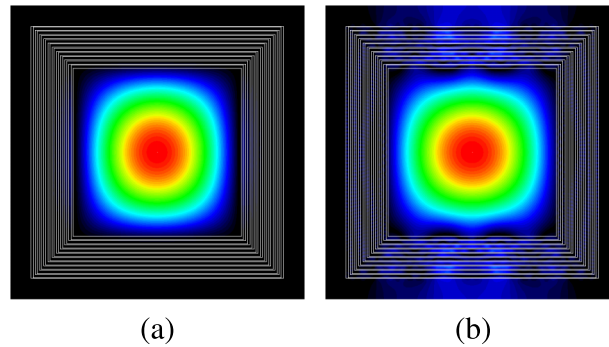


FIG. 12. Modal field of a single-polarization hollow-core square PBG waveguide consisting of a core with $a = b = 40\Lambda$ and a 10-period Bragg cladding ($d_{1x} = d_{2x} = 0.5\Lambda$, $d_{1y} = 0.8\Lambda$, and $d_{2y} = 0.2\Lambda$) at $\Lambda/\lambda = 0.24$. (a) x -polarized mode. (b) y -polarized mode.

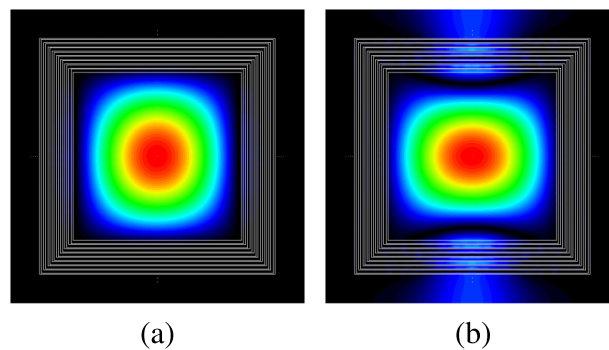


FIG. 13. Modal field of a single-polarization hollow-core square PBG waveguide consisting of a core with $a = b = 40\Lambda$ and an 8-period Bragg cladding ($d_{1x} = d_{2x} = 0.5\Lambda$, $d_{1y} = 0.8\Lambda$, and $d_{2y} = 0.2\Lambda$) at $\Lambda/\lambda = 0.24$. (a) x -polarized mode. (b) y -polarized mode.

of layer periods causes the stronger effect of periodic structure and thus leads to stronger Bragg reflections, but at the same time causes a decrease in the transmittance in the passband. As a result, even though the TM waves are out of their bandgap, the transmittance decrease would have resulted in intensifying their reflections in the y direction.

We thus consider decreasing the number of layer periods to 8 to recover the TM wave transmittance in the passband and show the modal field distribution of a single-polarization hollow-core square PBG waveguide with an 8-period Bragg cladding in Fig. 13. In the x -polarized mode, the light is well confined in the core, while in the y -polarized mode, the light leaks to the outside of the

TABLE I. Effective index of single-polarization hollow-core square photonic bandgap waveguides at $\Lambda/\lambda = 0.24$.

Periodic number	$N = 5$	$N = 8$	$N = 10$
k_z/k_0	0.997787	0.997321	0.997322

core through the Bragg cladding. This shows that the hollow-core square PBG waveguide shown in Fig. 13 provides single-polarization guiding that supports only the x polarization. Table I shows the effective indices of the x -polarized mode for each number of layer periods. These waveguides are found to have effective indices close to that of a metallic waveguide with the same size, which is 0.997284, compared with the hollow-core PBG waveguide guiding both polarizations mentioned in Section III. This seems to be because the x -polarized mode has similar modal field distributions in the x and y directions, as can be seen in Fig. 13(a).

We finally estimated the transmission loss of the HE_{11} mode in this hollow-core square PBG waveguide, using a vector finite-element beam propagation method.²⁷ As a result, the estimated loss value was approximately 0.04 dB/cm for the x -polarized mode HE_{11}^x whereas over 8 dB/cm for the y -polarized mode HE_{11}^y . The y -polarized mode suffers higher attenuation losses than the x -polarized mode and thus this waveguide was confirmed to be able to guide only x -polarized waves.

V. CONCLUSION

Summarizing, we have discussed hollow-core optical waveguides with a rectangular Bragg cladding consisting of periodically stratified dielectric films. These waveguides guiding hybrid modes can be designed based on the bandgap estimation of Bragg cladding using the approximated 1D periodic dielectric films stacked in the respective x and y directions; thus the polarization-dependent property of the PBG of 1D periodic multilayer structures has been systematically studied in detail. In order to use the polarization anisotropy of bandgap, the bandgap for TE waves excluding that for TM waves will be utilized. From the obtained results, we verified that the thicker low-index layer relative to the high-index layer and wave propagations with larger tangential wavenumbers lead to larger bandgap differences between the two polarized waves.

A hollow-core rectangular PBG waveguide was designed based on our design principle for the Bragg cladding and the fundamental mode was confirmed to be well confined in the core region. Moreover, we also proposed a novel hollow-core square PBG waveguide structure that enables single-polarization guiding, and demonstrated that the single-polarization guiding can be achieved by using the square Bragg cladding structure with different layer thickness ratios in the x and y directions. The BPM simulation demonstrated that the designed waveguide can be achieved with relatively low loss.

Although, with present-day technology, it would be difficult to precisely fabricate the hollow-core rectangular PBG waveguide with a Bragg cladding mentioned here, the application of the MCVF process for optical fiber fabrication to microtubes with micron-scale diameters or future progress in 3D printer technology will enable us to fabricate more complicated and finer structures.

APPENDIX A: THEORETICAL OVERVIEW: PBG OF FINITE PERIODIC MULTILAYER STRUCTURE

Let us now consider a multilayer dielectric stack composed of $2N$ layers, shown in Fig. 2(b). Each layer has a refractive index $n_i (i = 1, 2, \dots, 2N)$ and the media adjacent to both sides of the finite multilayer stack are assumed to be air ($n_0 = n_{2N+1} = 1$). Then the field components E_y and H_y for the TE and TM waves, respectively, propagating in the xz plane of the multilayer medium satisfy the wave equation

$$\frac{\partial^2}{\partial x^2} \Psi + (k_0^2 n^2 - k_z^2) \Psi = 0, \quad (\text{A1})$$

$$\Psi = \begin{cases} E_y & \text{for TE wave} \\ H_y & \text{for TM wave} \end{cases},$$

where k_0 is the free-space wavenumber, n is the refractive index of medium, k_z is the tangential component of the wavevector \mathbf{k} , and each layer is assumed to be homogeneous. The solutions of Eq. (A1) are of the form $\exp[j(\omega t - \mathbf{k} \cdot \mathbf{r})]$. Here the wave traveling in the positive z -direction and at an angle θ_i in the i th layer is assumed, and hence the wavevector is written by

$$\mathbf{k}_i = (\pm k_{x,i}, 0, k_z) = (\pm k_0 n_i \cos \theta_i, 0, k_0 n_i \sin \theta_i), \quad (\text{A2})$$

where $\pm k_{x,i}$ represents the wavenumber component along the stacking direction in the i th layer, and the upper and lower signs correspond to forward and backward propagating waves, respectively. $k_{x,i}$ is given by

$$k_{x,i} = \sqrt{k_0^2 n_i^2 - k_z^2}. \quad (\text{A3})$$

The wave equation (A1) has solutions of the form

$$\Psi_i(\bar{x}) = A \cos(k_{x,i} \bar{x}) + B \sin(k_{x,i} \bar{x}), \quad (\text{A4})$$

where $\bar{x} = x - x_i$.

Since the multilayer structure is taken to be uniform in both y and z directions, the tangential magnetic field component $H_{z,i}$ for TE (s) waves is obtained from Maxwell's equations:

$$H_{z,i}(\bar{x}) = \frac{k_{x,i}}{j\omega\mu_0} [A \sin(k_{x,i} \bar{x}) - B \cos(k_{x,i} \bar{x})], \quad (\text{A5})$$

where A and B are amplitude coefficients. Then, the tangential field components at the interfaces at $\bar{x} = 0$ and d_i are given by

$$E_{y,i}(0) = A, \quad (\text{A6})$$

$$H_{z,i}(0) = -\frac{k_{x,i}}{j\omega\mu_0} B, \quad (\text{A7})$$

$$E_{y,i}(d_i) = \cos \phi_i E_{y,i}(0) - \frac{j\omega\mu_0}{k_{x,i}} \sin \phi_i H_{z,i}(0), \quad (\text{A8})$$

$$H_{z,i}(d_i) = \frac{k_{x,i}}{j\omega\mu_0} \sin \phi_i E_{y,i}(0) + \cos \phi_i H_{z,i}(0), \quad (\text{A9})$$

$$\phi_i = k_{x,i} d_i = d_i k_0 n_i \cos \theta_i. \quad (\text{A10})$$

The matrix equation is obtained from Eqs. (A8) and (A9):

$$\begin{bmatrix} E_{y,i}(0) \\ H_{z,i}(0) \end{bmatrix} = \begin{bmatrix} \cos \phi_i & \frac{j \sin \phi_i}{\eta_i^s} \\ j \eta_i^s \sin \phi_i & \cos \phi_i \end{bmatrix} \begin{bmatrix} E_{y,i}(d_i) \\ H_{z,i}(d_i) \end{bmatrix}, \quad (\text{A11})$$

$$\eta_i^s = \frac{k_{x,i}}{\omega\mu_0} = \frac{n_i \cos \theta_i}{Z_0}, \quad (\text{A12})$$

where Z_0 and μ_0 are the wave impedance and the permeability, respectively, of free space.

For TM waves, we can obtain the matrix equation by the same arguments as before.

$$\begin{bmatrix} -E_{z,i}(0) \\ H_{y,i}(0) \end{bmatrix} = \begin{bmatrix} \cos \phi_i & \frac{j \sin \phi_i}{\eta_i^p} \\ j \eta_i^p \sin \phi_i & \cos \phi_i \end{bmatrix} \begin{bmatrix} -E_{z,i}(d_i) \\ H_{y,i}(d_i) \end{bmatrix}, \quad (\text{A13})$$

$$\eta_i^p = \frac{k_{x,i}}{\omega\epsilon} = \frac{n_i}{Z_0 \cos \theta_i}. \quad (\text{A14})$$

Designating the tangential electromagnetic field components at the interface i as e_i and h_i , and applying Eq. (A11) or (A13) iteratively, we can relate the amplitudes e_1 and h_1 at the beginning face

to those e_{2N+1} and h_{2N+1} at the end face by the transfer matrix M .

$$\begin{bmatrix} e_1 \\ h_1 \end{bmatrix} = [M] \begin{bmatrix} e_{2N+1} \\ h_{2N+1} \end{bmatrix}, \quad (\text{A15})$$

$$[M] = \prod_{i=1}^{2N} [M_i], \quad (\text{A16})$$

$$[M_i] = \begin{bmatrix} \cos \phi_i & \frac{j \sin \phi_i}{\eta_i^\xi} \\ j\eta_i^\xi \sin \phi_i & \cos \phi_i \end{bmatrix}, \quad (\xi = s \text{ or } p). \quad (\text{A17})$$

The transmission coefficient is given by¹⁸

$$T = \frac{\eta_{2N+1}^\xi}{\eta_0^\xi} |\tau|^2, \quad (\text{A18})$$

$$\tau = \frac{2\eta_0^\xi}{\eta_0^\xi(M_{11} + \eta_{2N+1}^\xi M_{12}) + M_{21} + \eta_{2N+1}^\xi M_{22}}, \quad (\text{A19})$$

where M_{ij} represents the (i, j) element of the transfer matrix M .

In the present study, we consider finite periodic multilayer stacks composed of $2N$ layers with refractive indices and thicknesses of

$$(n_i, d_i) = \begin{cases} (n_1, d_1) & \text{for odd } i \\ (n_2, d_2) & \text{for even } i \end{cases}. \quad (\text{A20})$$

The number of layer periods N corresponds to the number of unit cells.

APPENDIX B: THEORETICAL OVERVIEW: PBG OF INFINITE PERIODIC MULTILAYER STRUCTURE

Figure 2(a) shows one period of an infinite periodic multilayer medium with a period of length $\Lambda = d_1 + d_2$ corresponding to a unit cell. Here, \bar{x} is replaced by x in Eqs. (A4) and (A5), and the interface between two layers is taken at $x = 0$. Obliquely propagating waves on the xz plane satisfy the wave equation (A1). For a unit cell ($-d_1 \leq x \leq d_2$), using the Bloch-Floquet theorem, we can write the periodic boundary condition in the form

$$\Psi_{y,1}(-d_1) = \Psi_{y,2}(d_2) \exp(jK_x \Lambda), \quad (\text{B1})$$

$$p_1 \frac{\partial \Psi_{y,1}}{\partial x} \Big|_{x=-d_1} = p_2 \frac{\partial \Psi_{y,2}}{\partial x} \Big|_{x=d_2} \exp(jK_x \Lambda), \quad (\text{B2})$$

where K_x represents the wavenumber propagating in the periodic structure, which is referred to as the Bloch wavenumber, and $p_i = 1$ and $1/n_i^2$ for TE and TM modes, respectively. The requirements of continuity of the tangential field components at the interface $x = 0$ between two layers, and Eqs. (B1) and (B2) lead to the eigenvalue equation²⁰

$$\begin{aligned} \cos(K_x \Lambda) &= \frac{1 + \Omega}{2} \cos(\kappa_1 d_1 + \kappa_2 d_2) \\ &+ \frac{1 - \Omega}{2} \cos(\kappa_1 d_1 - \kappa_2 d_2), \end{aligned} \quad (\text{B3})$$

where

$$\Omega = \frac{p_1^2 \kappa_1^2 + p_2^2 \kappa_2^2}{2p_1 p_2 \kappa_1 \kappa_2}, \quad (\text{B4})$$

$$\kappa_i = \sqrt{k_0^2 n_i^2 - k_z^2}, \quad (i = 1, 2). \quad (\text{B5})$$

- ¹ J.C. Knight, T.A. Birks, P.St.J. Russell, and D.M. Atkin, *Opt. Lett.* **21**, 1547 (1996); Errata, *ibid.* **22**, 484 (1997).
- ² J. Broeng, D. Mogilevstev, S.E. Barkou, and A. Bjarklev, *Opt. Fiber Technol.* **5**, 305 (1999).
- ³ P. Yeh, A. Yariv, and E. Marom, *J. Opt. Soc. Am.* **68**, 1196 (1978).
- ⁴ Y. Fink, D.J. Ripin, S. Fan, C. Chen, J.D. Joannopoulos, and E.L. Thomas, *J. Lightwave Technol.* **17**, 2039 (1999).
- ⁵ S. Guo, S. Albin, and R.S. Rogowski, *Opt. Express* **12**, 198 (2004).
- ⁶ S.E. Barkou, J. Broeng, and A. Bjarklev, *Opt. Lett.* **24**, 46 (1999).
- ⁷ R.F. Cregan, B.J. Mangan, J.C. Knight, T.A. Birks, P.St.J. Russell, P.J. Roberts, and D.C.Allan, *Science* **285**, 1537 (1999).
- ⁸ J. Broeng, S.E. Barkou, T. Søndergaard, and A. Bjarklev, *Opt. Lett.* **25**, 96 (2000).
- ⁹ A. Ferrando and J.J. Miret, *Appl. Phys. Lett.* **78**, 3184 (2001).
- ¹⁰ M. Szpulak, T. Martynkien, J. Olszewski, W. Urbanczyk, T. Nasilowski, F. Berghmans, and H. Thienpont, *Acta Physica Polonica A* **111**, 239 (2007).
- ¹¹ Arismar Cerqueira S, Jr., D.G. Lona, I. de Oliveira, H.E. Hernandez-Figueroa, and H.L. Fragnito, *Opt. Lett.* **36**, 133 (2011).
- ¹² M. Eguchi and Y. Tsuji, *J. Lightwave Technol.* **31**, 177 (2013).
- ¹³ M.J. Steel, T.P. White, C.M. de Sterke, R.C. McPhedran, and L.C. Botten, *Opt. Lett.* **26**, 488 (2001).
- ¹⁴ T. Miura, F. Koyama, and A. Matsutani, *Jpn J. Appl. Phys.* **41**, 4785 (2002).
- ¹⁵ Y. Yi, S. Akiyama, P. Bermel, X. Duan, and L.C. Kimerling, *Opt. Express* **12**, 4775 (2004).
- ¹⁶ Y. Yi, S. Akiyama, P. Bermel, X. Duan, and L.C. Kimerling, *J. Sel. Top. Quantum Electron.* **12**, 1345 (2006).
- ¹⁷ G.R. Hadley, J.G. Fleming, and S.-Y. Lin, *Opt. Lett.* **29**, 809 (2004).
- ¹⁸ M. Born and E. Wolf, *Principles of Optics* (MacMillan, New York, 1964).
- ¹⁹ H.A. Macleod, *Thin-Film Optical Filters*, 4th ed. (CRC Press, 2010).
- ²⁰ P. Yeh, A. Yariv, and C.-S. Hong, *J. Opt. Soc. Am.* **67**, 423 (1977).
- ²¹ J.N. Winn, Y. Fink, S. Fan, and J.D. Joannopoulos, *Opt. Lett.* **23**, 1573 (1998).
- ²² Y. Fink, J.N. Winn, S. Fan, C. Chen, J. Michel, J.D. Joannopoulos, and E.L. Thomas, *Science* **282**, 1679 (1998).
- ²³ X. Wang, X. Hu, Y. Li, W. Jia, C. Xu, X. Liu, and J. Zi, *Appl. Phys. Lett.* **80**, 4291 (2002).
- ²⁴ D.N. Chigrin, A.V. Lavrinenko, D.A. Yarotsky, and S.V. Gaponenko, *J. Lightwave Technol.* **17**, 2018 (1999).
- ²⁵ M. Koshiba and Y. Tsuji, *J. Lightwave Technol.* **18**, 737 (2000).
- ²⁶ E.A.J. Marcatili, *Bell Syst. Tech. J.* **48**, 2071 (1969).
- ²⁷ Y. Tsuji and M. Koshiba, *J. Sel. Top. Quantum Electron.* **6**, 163 (2000).